Synthesis, Structure and Properties of Scandium Dysprosium Antimonide, ScDySb

Jürgen Nuss, Ulrich Wedig, Martin Jansen

Zeitschrift für Anorganische und Allgemeine Chemie

Synthesis, Structure and Properties of Scandium Dysprosium Antimonide, ScDySb

Journal:	*Zeitschrift für Anorganische und Allgemeine Chemie*
Manuscript ID:	zaac.201000095
Wiley - Manuscript type:	Article
Date Submitted by the Author:	18-Feb-2010
Complete List of Authors:	Nuss, Jürgen; MPI für Festkörperforschung, Chemie III Wedig, Ulrich; MPI für Festkörperforschung, Chemie III Jansen, Martin; MPI für Festkörperforschung
Keywords:	Ternary pnictides, Metal-metal interactions, Crystal structures, Magnetic properties, ELF (Electron Localization Function)

ARTICLE

DOI: 10.1002/zaac.200((will be filled in by the editorial staff))

Synthesis, Structure and Properties of Scandium Dysprosium Antimonide, ScDySb

Jürgen Nuss,[a] Ulrich Wedig,[a] and Martin Jansen*[a]

Dedicated to Professor Rüdiger Kniep on the Occasion of His 65th Birthday

Keywords: Ternary pnictides; Metal-metal interactions; Crystal structures; Magnetic properties; ELF (Electron Localization Function); Density functional calculations

Abstract. Scandium dysprosium antimonide ScDySb was synthesized from scandium metal and DySb in an all-solid state reaction at 1770 K. According to X-ray analysis of the crystal structure (*P*4/*nmm*, *Z* = 4, *a* = 430.78(1) pm, *c* = 816.43(4) pm, R_1 = 0.0238, *wR*(all) = 0.0688, 268 independent reflections), ScDySb adopts the *anti*-PbFCl type of structure, but with pronounced deviations in structural details, which are related to specific bonding interactions between the atoms involved. ScDySb shows antiferromagnetic ordering below 35.4 K, which was verified by susceptibility, heat capacity, and resistivity measurements. X-ray structure determination, performed at 30 K, showed no significant structural changes to occur during the magnetic phase transition. The band structure has been calculated in the framework of Density Functional Theory. The bonding properties are comparable to those of Sc_2Sb. Pronounced basins of the Electron Localization Function (ELF) appears in the tetragonal pyramidal Sc_4Dy voids.

* Prof. Dr. M Jansen
Fax: +49-711-689-1502
E-mail: M.Jansen@fkf.mpg.de
[a] Max-Planck-Institut für Festkörperforschung
Heisenbergstr. 1
70569 Stuttgart, Germany

Introduction

The PbFCl type of structure is preferably and most frequently formed by ionic compounds with the formula *MXY*. Usually a large cation *M*, and two anions *X* and *Y*, which differ in size significantly, are the constituents needed. Representative members are fluoride- [1], oxide- [2, 3], hydride- [4], and nitride-halides [5]. However, if different kinds of interactions, like covalent or metallic bonding gain more importance, considerations based on a simple hard sphere model are no longer appropriate for respective compounds with this structure type. Numberless examples of the same atomic arrangement with partial covalent or metallic bonding have been reported. Among them are ZrSiS [6, 7] or NbSiAs [8], and also intermetallic phases of general formula A_2B (*A*1*A*2*B*). In the latter case, one (*A*), or two different metals (*A*1, *A*2) occupy the sites of F and Cl in PbFCl, while a metalloid (*B*), which is often a heavy element of group 14 or 15, substitute for Pb. Some interesting representatives of such *anti*-PbFCl type structures are: Cu_2Sb [9], Fe_2As [10], Sc_2Sb [11], LiFeAs [12, 13], Ti*RE*Ge (*RE* = Y, Gd-Tm) [14].

All in all, about 990 compounds are referred to crystallize in the PbFCl (*anti*-PbFCl) type of structure [15, 16]. The structural variations caused by varying bonding principles can be fully addressed by only two parameters, the *c*/*a* ratio of the tetragonal crystal system and the ratio of the two free atomic parameters (z_{Pb} and z_{Cl} for PbFCl). Recently, we have presented a structure map, which allows for identifying ionic, covalent, and metallic bonding regions among all the (*anti*) PbFCl type representatives [9, 10].

Sc_2Sb [11] was the first example showing the general topology of PbFCl where pronounced basins of the Electron Localisation Function (ELF) was found in the square pyramidal voids [10]. Since such structural and electronic features can be regarded a prerequisite for interesting phenomena, we are looking for further compounds with the same phenotype. Here we report on synthesis and characterisation of a new representative: ScDySb, which is the only representative in the series Sc*RE*Sb (*RE* = rare earth metal) crystallizing in the PbFCl type of structure, known up to now. The other members (*RE* = La, Ce, Pr, Nd, Sm, Tb) all adopt the La_2Sb structure type [17].

Results and Discussion

Starting from binary DySb and scandium metal, the compound ScDySb has been synthesized by all-solid state reaction as a silver grey regulus in gram amounts, and as a single phase product.

Physical Properties

The temperature variation of the magnetic susceptibility, $\chi(T)$, shows *Curie-Weiss* behaviour at higher temperatures (200-330 K, Figure 1). Data analysis result in an effective magnetic moment (μ_{eff}) of 10.75 μ_B, which is very close to the expectation value for the $^6H_{15/2}$ ground state configuration of the Dy^{3+} ion (10.65 μ_B) and a *Curie-Weiss* temperature θ_w of +32 K. The positive θ_w value indicates ferromagnetic interaction to dominate at higher temperatures, while antiferromagnetic ordering occurs at T_N = 35 K (Figure 1).

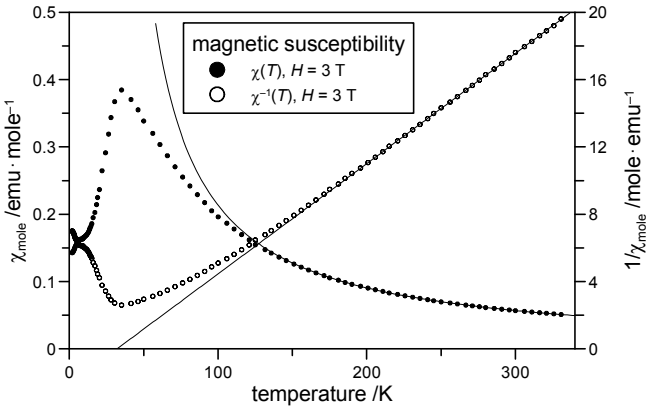

Figure 1. Susceptibility and inverse susceptibility of ScDySb versus temperature.

The specific resistivity, $\rho(T)$, of ScDySb drops almost linearly between 295 K (1.25 mΩ·cm) and 50 K (0.87 mΩ·cm), which corresponds to a typical metallic behaviour. Near 35 K, the resistivity exhibits an anomaly which is due to the onset of the magnetic ordering (Figure 2).

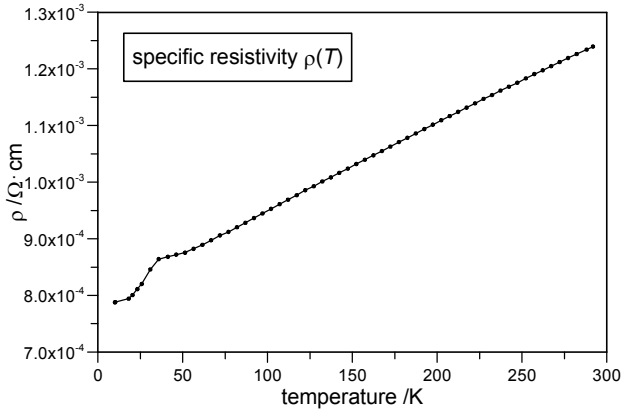

Figure 2. Electric resistivity vs. temperature of ScDySb, between 5 and 295 K.

Temperature dependence of the heat capacities, $C_p(T)$, of ScDySb in applied fields of 0 and 7 T are presented in Figure 3. A sharp peak is observed in zero-field heat capacity at 35.4 K, which coincides with the antiferromagnetic ordering temperature of the compound.

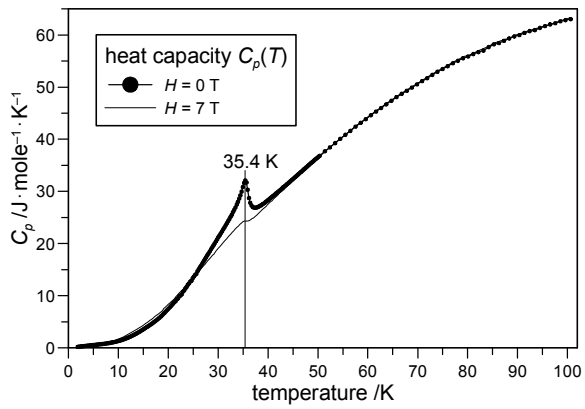

Figure 3. Heat capacity of SyDySb, between 2 and 100 K.

In order to verify whether the magnetic ordering at 35.4 K is accompanied by a structural phase transition, single crystals were measured at room temperature and 30 K (Table 1-3). No significant structural changes were observed at low temperatures, except for a decrease of lattice constants and displacement parameters, which is a result of the reduced thermal motion. The absence of structural chemical changes is not atypical, as can be seen using the example of the antiferromagnetic transition of isotypic TiTbSi [14, 18], where neutron diffraction studies [18] indicate that the magnetic structure consists of ferromagnetic Tb double layers which are antiferromagnetically coupled along the *c*-axis, a picture, which seems to be consistent with the magnetic properties of ScDySb as well.

Crystal Structure

According to a single crystal X-ray diffraction analysis, ScDySb crystallizes in the tetragonal *anti*-PbFCl type of structure (space group *P*4/*nmm*, Pearson code *tP*6, Wyckoff sequence *c*2*a*), with dysprosium and antimony occupying the two 2*c* sites (¼, ¼, *z*), while scandium is located on the special position 2*a* (¾, ¼, 0), c.f. Tables 1-3.

Table 1. Crystal data, data collection, and refinement details for ScDySb.

Temperature /K	296.0(2)	30.0(2)
Formula weight	329.21	
Space group (no.), *Z*	*P*4/*nmm* (129), 2	
Lattice constants /pm	a = 430.78(1)	429.99(7)
	c = 816.43(4)	812.94(14)
	c/a = 1.895	1.891
V /Å^3,	151.51(1)	151.31(4)
ρ_{xray} /g cm^{-3}	7.216	7.274
Crystal size	0.040×0.025×0.015	
Diffractometer	SMART APEX II, Bruker AXS	
X-ray radiation, λ /Å	0.71073	
Absorption correction	multi-scan, SADABS [29]	
2θ range /°	$4.98 \le 2\theta \le 74.34$	
Index range	$-7 \le h \le 7$,	
	$-7 \le k \le 7$,	
	$-13 \le l \le 13$	
Reflection collected	3991	3747
Data, R_{int}	268, 0.020	268, 0.032
No. of parameters	10	
Transmision: t_{max}, t_{min}	0.621, 0.334	0.619, 0.332
$R_1[F^2 > 2\sigma(F^2)]$	0.0238	0.0252
$wR(F^2)$	0.0688	0.0722
Extinction coefficient	0.0063(16)	0.0063(18)
Deposition no. [32]	CSD-421439	CSD-421440

Table 2. Atomic coordinates and displacement parameters U_{ij} /pm^2 for ScDySb at 30 and 296 K ($U_{12} = U_{13} = U_{23} = 0$).

Table 2 in two-column format, see end of file

Table 3. Interatomic distances /pm in ScDySb at 30 and 296 K.

Atomic contact		distance 296 K	30 K	mult.
Dy	— Sb	310.8(1)	309.8(1)	1
		311.76(2)	311.08(5)	4
	— Sc	358.06(4)	356.56(6)	4
Sb	— Dy	310.8(1)	309.8(1)	1
		311.76(2)	311.08(5)	4
	— Sc	307.63(6)	306.66(6)	4
Sc	— Dy	358.06(4)	356.56(6)	4
	— Sb	307.63(6)	306.66(6)	4
	— Sc	304.61(1)	304.05(5)	4

The strongly bonded hetero-atomic framework $^{3}_{\infty}[SbDy_{5/5}Sc_{4/4}]$ is formed by condensed $SbDy_5Sc_4$ monocaped square antiprisms [*d*(Sb—Dy) = 310.8(1) pm (×1), *d*(Sb—Dy) = 311.76(2) pm (×4), *d*(Sb—Sc) = 307.63(6) pm (×4), c.f. Table 3 and Figure 4a], which, of course, is also a distinguished feature of PbFCl (Figure 4b). The nearest neighbours of dysprosium are five Sb atoms arranged at the corners of a square pyramid, thus forming NaCl type fragments, which are also present in La_2Sb and related structures [17, 19, 20]. ScDySb is a shear variant of the *tI*12 structure type of La_2Sb (shear vector ½ ½ 0). The much shorter *d*(Sc—Sc) distance of 304.51(1) pm in comparison to *d*(Sc—Dy) = 358.06(4) pm, in the non-capped square of the $SbDy_5Sc_4$ polyhedra, indicate additional Sc—Sc interactions in the 4^4 nets of Sc (see Figure 4a). The distances *d*(Sc—Sc) are the shortest distances in the structure, shorter than *d*(Sc—Sb) = 307.63(6), and even shorter than in metallic scandium (321.2 pm). Similar structural relationships are found in Sc_2Sb [11]. Thus ScDySb can be regarded as a layered structure with alternating Sc 4^4 nets and rock-salt like double layers of DySb [9, 10], see Figure 4a.

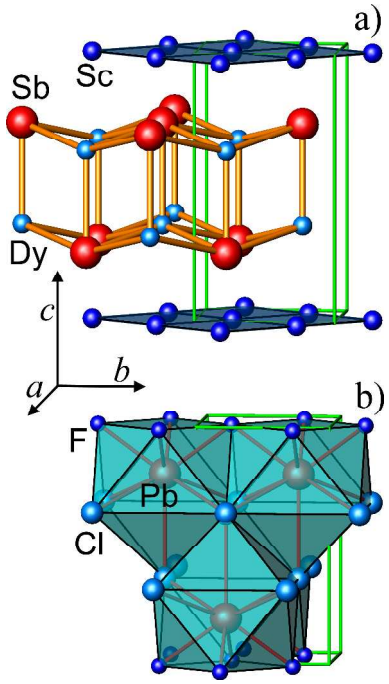

Figure 4. Perspective representation of the crystal structures of a) ScDySb and b) PbFCl. The margins of the unit cell are shown in green, [37].

The structural relationships of all PbFCl type representatives can be described illustratively by plotting the ratio of the site parameters $q = z_{A2}/(1-z_B)$ against the *c*/*a* ratio (*p*), with A2 = Dy and B = Sb for e.g. ScDySb, see Figure 5. At the first glance, this choice of coordinates for a structural field diagram seems to be rather arbitrary, but the representation allows to distinguish the interactions between A1—B, A2—B, and A1—A2 (*q*) in comparison to the A1—A1 interactions, the latter ones being represented by *c*/a (*p*). Of course, this works only when the crystallographic origin and the crystallographic sites of the respective atoms correspond. This is described in detail in [9] and [10]. As expected, ScDySb can be found in the same region of the structure field as Sc_2Sb, showing the same structural relations as described above (Figure 5).

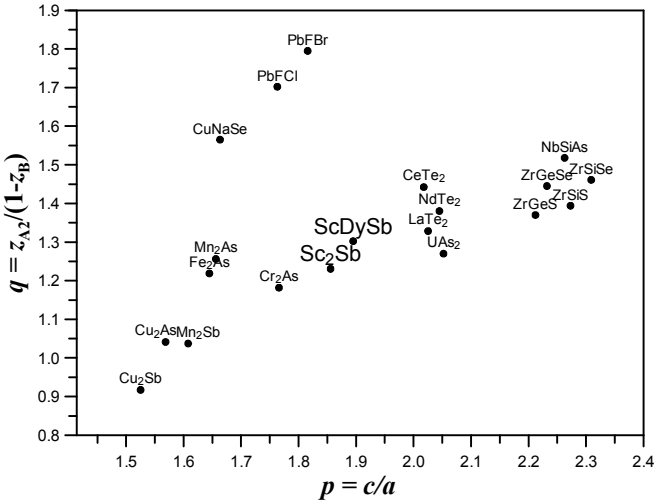

Figure 5. Structure map, showing selected A_2B compounds. The function $z_{A2}/(1-z_B) = f(c/a)$ visualizes the structural distortion (data from [9-11, 16]).

Electronic Structure

The band structure calculations reveal the similarity of the electronic structures of ScDySb and Sc_2Sb. Disregarding the Dy 4*f* bands, the densities of states (DOS) and their atom- and *l*-dependent projections show the same features (c.f. [10] and Figure 6). Rather broad bands with mainly Sb 5*p* character start at 1.2 eV below the Fermi level (E_F). These are separated from the bands around E_F, which show the character of the Sc and Dy valence orbitals. Remarkable are very narrow bands at –0.7 eV. Like in Sc_2Sb they can be pulled together with the interstitial localization pattern discussed below. The only significant difference between the band structures of the two compounds is the spin polarization in ScDySb originating from the partially filled 4*f* shell of Dy. The integrated spin density within the Dy atomic sphere amounts to 4.6 electrons. This is consistent with a hextet Dy^{3+} ground state as deduced from the magnetic measurements. The spin polarization on the other atomic sites is negligible. A ferromagnetic ordering within the DySb double layers is by 10 kJ/mole more stable than an antiferromagnetic one. Coupling adjacent ferromagnetic double layers antiferromagnetically leads to a further gain of 2 kJ/mole. Although the energy differences are rather small, assuming a magnetic ordering as found in TiTbSi [18] appears reasonable.

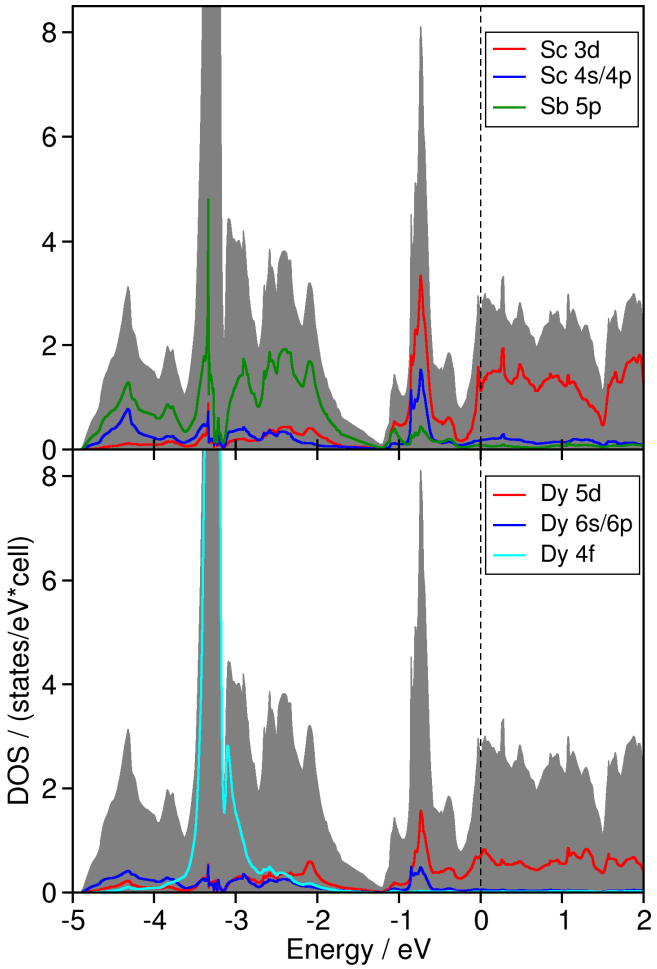

Figure 6. Total (grey area) and projected densities of states (see legend) of the majority spin component of ScDySb. The Fermi level (E_F) is shifted to 0 eV.

The substitution of Sc2 in Sc_2Sb by Dy leads to an increase of the unit cell volume by 9.3 %. According to the results of the topological analysis of the computed electron density, this is due to the Dy atomic basin, which is by 27.9 % larger than the corresponding Sc2 basin. The Sc (Sc1) and the Sb basins are expanded by only 4.4 % and 2.6 % respectively. The variation of the charges in the basins is in the order of only 0.1 electrons. The more pronounced buckling of the double layers and the enhanced *c/a* ratio in ScDySb and thus the slight different position in the structure map (Fig. 5), as compared to Sc_2Sb, seems to have primarily no electronic origin, but is due to the space requirements of the dysprosium atom.

The expansion of the unit cell leads to a slight shrinkage (10.5 $Å^3$ vs. 10.7 $Å^3$ in Sc_2Sb) of that basin of the Electron Localization Function (ELF, [21]), which is situated in the tetragonal pyramidal voids enclosed by four Sc and one Dy atoms (Figure 7). The integrated valence electron density within this basin amounts to 1.2 electrons. Careful analysis of the final difference Fourier map gave no evidence for an interstitial atom in these Sc_4Dy cavities, which one might expect to be present in analogy to previous instances when overlooked interstitial atoms were identified by localization patterns [22]. Such stuffed intermetallics are known however, in the series $RE_9Sb_5O_5$ (*RE* = La, Ce, Pr, Sm, Tb, Dy) [23-25], where oxygen occupies corresponding voids in this type of structure, which can also be regarded as a stuffed defect variant of Sc_2Sb [23] and therefore of ScDySb, too: $[Dy_5Sb_5][Sc_5\square_5] \triangleq [RE_5Sb_5][RE_4\square O_5]$.

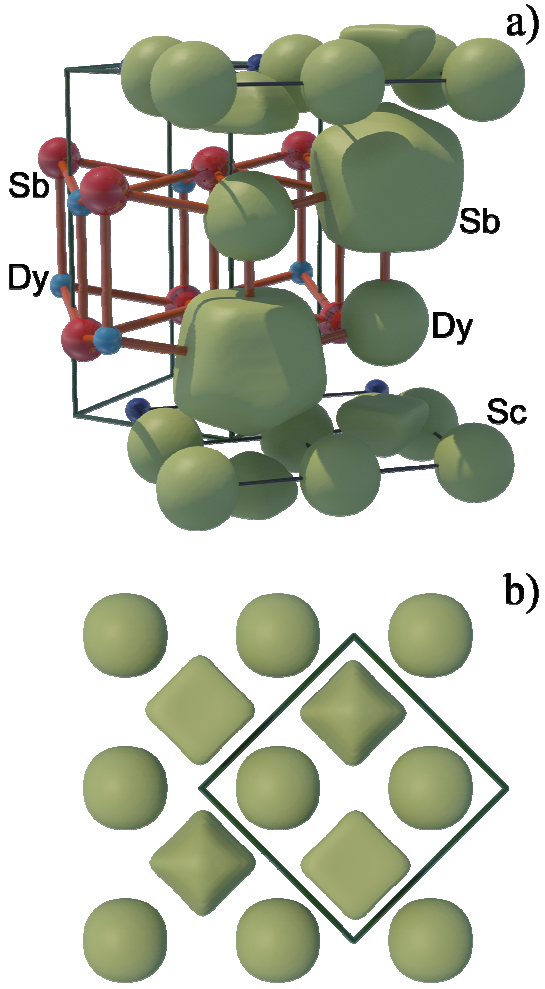

Figure 7. Domains of the Electron Localization Function (ELF, η = 0.5) in ScDySb, a) perspective representation of the crystal structure, b) Sc-layer perpendicular to the *c*-axis.

Conclusions and Outlook

Based on a thorough analysis of ScDySb, we claim that the localisation pattern found in the voids is an intrinsic property of the ELF topology in this intermetallic compound, indicating a multi centre interaction between the metal atoms. ScDySb is a further example showing this pronounced topology, and confirms the feature previously reported for Sc_2Sb [10]. This special relation is also reflected by the position of both compounds in the discussed structure field diagram (Figure 5).

The structure of ScDySb, and also the structure of other *anti*-PbFCl representatives, show atomic arrangements, which are closely related to the La_2Sb type of structure. Both can be transferred into each other by a virtual shearing (shear vector ½ ½ 0), whereby the most pronounced structural changes are affected to the pyramidal voids, which change into octahedral ones in the case of La_2Sb. A stuffed variant, e.g. Eu_4Sb_2O [19], is known, where these voids are occupied by oxygen. An analogue stuffed variant of Sc_2Sb type compounds is still missing. It is amazing, that all the other representatives Sc*RE*Sb with larger rare earth elements

(*RE* = La, Ce, Pr, Nd, Sm, Tb) are known to adopt the La_2Sb type of structure [17]. The relationship between 'empty' and 'filled' La_2Sb type compounds and their differences in the electronic properties will be discussed somewhere else [26].

Experimental Section

Synthesis: ScDySb was synthesized in ~1 g batches from DySb and scandium metal (ChemPur, Karlsruhe, Germany). The binary dysprosium antimonide was prepared from the elements in a sealed tantalum ampoule at 1120 K for 36 h. In order to remove potential impurities of hydrogen, the reaction was done in dynamic vacuum (10^{-4} mbar). Stoichiometric amounts of the starting materials were mixed and sealed in a tantalum ampoule. The following temperature profile was applied: 298 → 1770 K (50 K h^{-1}, subsequent annealing for 36 h); 1770 → 1520 K (25 K h^{-1}, subsequent annealing for 60 h); 1520 → 298 K (50 Kh^{-1}).

Physical properties: Magnetic susceptibility $\chi(T)$ of a powder sample of about 40 mg was measured with a Quantum Design Magnetic Properties Measurements System (MPMS). The susceptibility was recorded at H = 0.001, 0.1, 1, 3 and 7 T in the temperature range of 2-330 K. The heat capacity $C_p(T)$ was determined with a Quantum Design Physical Properties Measurement System (PPMS) in the temperature range of 2-100 K at H = 0, 0.1, 3 and 7 T. Both systems manufactured by Quantum Design, San Diego, CA. Temperature dependent resistivity has been obtained for pressed pellets using the *van der Pauw* method [27] (5-295 K at 5 K intervals).

Structure determination: The diffraction data were collected at 30 and 296 K on a SMART-APEX-II CCD X-ray diffractometer (Bruker AXS, Karlsruhe, Germany) with graphite-monochromated Mo$K\alpha$ radiation, equipped with a N-Helix low temperature device [Oxford Cryosystems, Oxford, United Kingdom (28-300 K)] [28]. The reflection intensities were integrated with the SAINT subprogram in the Bruker Suite software package [29], a multi-scan absorption correction was applied using SADABS [30]. The structures were solved by direct methods and refined by full-matrix least squares fitting with the SHELXTL software package [31]. Experimental details are given in Tables 1 and 2. Further details may be obtained from Fachinformationszentrum Karlsruhe [32].

Band structure calculations: Scalar relativistic density functional calculations (DFT) were performed with the TB-LMTO-ASA program [33], applying the local spin density approximation (LSDA) to allow for spin polarization. The local exchange-correlation functional of v. Barth and Hedin [34] was used. The Kohn-Sham eigenvalues were computed at 140 irreducible *k*-points in the Brillouin zone. In addition to the atomic spheres, empty spheres were added at Wyckoff position 2*b* (¼ ¾ ½) in order to enable the neglect of the interstitial region and to reduce the overlap of the atomic spheres. Supercells (2***a***×***b***×***c*** and ***a***×***b***×2***c***) were considered to investigate the spin ordering.

The Electron Localization Function (ELF), derived from the Pauli kinetic energy density [21], was computed as an indicator for local electronic substructures like core shells, covalent bonds and lone pairs. Both, the total electron density and the ELF were investigated by a topological analysis [35, 36], separating the whole space into atomic or localization basins. The charges within these basins were computed by integrating the valence electron density, being available in a regular mesh with a grid distance of 7 pm.

Acknowledgments

The authors gratefully acknowledge the help of Mrs. *S. Prill-Diemer* for carrying out the synthesis, Mrs. *E. Brücher* for susceptibility measurements, and Mrs. *G. Siegle* for resistivity and heat capacity measurements. This work was supported by the Deutsche Forschungsgemeinschaft (DFG) within the priority program *Experimental charge density as the key to understand chemical interaction* (SPP1178).

References

[1] H. P. Beck, *Z. Anorg. Allg. Chem.* **1979**, *415*, 73.

[2] H. Bärnighausen, *J. Prakt. Chem.* **1961**, *14*, 313.

[3] H. Bärnighausen, G. Brauer, N. Schultz, *Z. Anorg. Allg. Chem.* **1965**, *338*, 250.

[4] H. P. Beck, A. Limmer, *Z. Anorg. Allg. Chem.* **1983**, *502*, 185.

[5] R. Juza, K. Meyer, *Z. Anorg. Allg. Chem.* **1969**, *366*, 43.

[6] A. J. Klein Haneveld, F. Jellnik, *Rec. Trav. Chim. Pays-Bas* **1964**, *83*, 776.

[7] H. Onken, K. Vierheilig, H. Hahn, *Z. Anorg. Allg. Chem.* **1964**, *333*, 267.

[8] V. Johnson, W. Jeitschko, *J. Solid State Chem.* **1973**, *6*, 306.

[9] J. Nuss, M. Jansen, *Z. Anorg. Allg. Chem.* **2002**, *628*, 1152.

[10] J. Nuss, U.Wedig, M Jansen, *Z. Kristallogr.* **2006**, *221*, 554.

[11] J. Nuss, M. Jansen, *Z. Kristallogr. NCS.* **2002**, *217*, 19.

[12] X. C. Wang, Q. Q. Liu, Y. X. Lv, W. B. Gao, L. X. Yang, R. C. Yu, F. Y. Li, C. Q. Jin, *Solid State Comm.* **2008**, *148*, 538.

[13] J. H. Tapp, Z. Tang, B. Lv, K. Sasmal, B. Lorenz, P. C. W. Chu, A. M. Guloy, *Phys. Rev. B* **2008**, 060505(R).

[14] A. V. Morozkin, Y. D. Seropegin, A. V. Leonov, I. A. Sviridov, I. A. Tskhadadze, S. A. Nikitin, *J. Alloys. Comp.* **1998**, *267*, L14.

[15] Inorganic Crystal Structure Database (ICSD) Fachinformationszentrum (FIZ) Karlsruhe **2009**.

[16] P. Villars, K. Cenzual, Pearson's Crystal Data: Crystal Structure Database for Inorganic Compounds, Release 2009/10, ASM International®, Materials Park, Ohio, USA **2009**.

[17] J. Nuss, M. Jansen, paper in progress.

[18] A. V. Morozkin, A. I. Kurbakov, *J. Alloys. Comp.* **2002**, *345*, L4.

[19] H. Schaal, J. Nuss, W. Hönle, Yu. Grin, H. G. von Schnering, *Z. Kristallogr. NCS* **1998**, *213*, 15.

[20] W. N. Stassen, M. Sato, L. D. Calvert, *Acta Crystallogr.Sect. A* **1970**, *26*, 1534.

[21] A. Savin, O. Jepsen, J. Flad, O. K. Andersen, H. Preuss, H. G. von Schnering *Angew. Chem. Int. Ed. Engl.* **1992**, *31*, 187; *Angew. Chem.***1992**, *104*, 186.

[22] R. Nesper, S. Wengert, *Chem. Eur. J.* **1997**, *3*, 985.

[23] J. Nuss, H. G. von Schnering, Y. Grin, *Z. Anorg. Allg. Chem.* **2004**, *630*, 2287.

[24] J. Nuss, M. Jansen, *Acta Crystallogr., Sect. B: Struct. Sci.* **2007**, *63*, 843.

[25] J. Nuss, M. Jansen, *Z. Kristallogr. NCS* **2009**, *224*, 11.

[26] J. Nuss, U. Wedig, M. Jansen, paper in progress.

[27] L.J. van der Pauw, *Philips Res. Rep.* **1958**, *13*, 1.

[28] G. Cakmak, J. Nuss, M. Jansen, *Z. Anorg. Allg. Chem.* **2009**, *635*, 631.

[29] Bruker Suite, Version 2008/3, Bruker AXS Inc., Madison, USA **2008**.

[30] G. M. Sheldrick, SADABS — *Bruker AXS area detector scaling and absorption*, Version 2008/1, University of Göttingen, Germany **2008**.

[31] G. M. Sheldrick, *Acta Crystallogr., Sect. A: Found. Crystallogr.* **2008**, *64*, 112.

[32] Further details may be obtained from Fachinformationszentrum Karlsruhe, 76344 Eggenstein-Leopoldshafen, Germany (fax: (+49)-7247-808-666; e-mail: crysdata(at)fiz-karlsruhe.de, http://www.fiz-karlsruhe.de/request for deposited data.html) on quoting the CSD number: CSD-421439 and CSD-421440.

[33] R. W. Tank, O. Jepsen, A. Burkhardt, O. K. Andersen, TB-LMTO-ASA Version 4.7, Max-Planck-Institut für Festkörperforschung, Stuttgart, Germany **1998**.

[34] U. von Barth, L. Hedin *J. Phys. C* **1972**, *5*, 1629.

[35] R. F. W. Bader *Atoms in Molecules: a Quantum Theory*, Oxford University Press, Oxford, **1990**.

[36] B. Silvi, A. Savin *Nature* **1994**, *371*, 683.

[37] Dowty, E.: ATOMS — *a complete program for displaying atomic structures*, version 6.3.4, Shape Software, Kingsport, USA **2008**.

Received: ((will be filled in by the editorial staff))
Published online: ((will be filled in by the editorial staff))

Table 2. Atomic coordinates and displacement parameters U_{ij} /pm^2 for ScDySb at 30 and 296 K ($U_{12} = U_{13} = U_{23} = 0$).

Atom	Site	*x*	*y*	*z*	$U_{11} = U_{22}$	U_{33}	U_{eq}	*T* /K
Dy	2*c*	¼	¼	0.35035(6)	94(2)	102(2)	97(2)	296
				0.34991(6)	45(3)	62(2)	50(2)	30
Sb	2*c*	¼	¼	0.73097(9)	86(2)	120(3)	98(2)	296
				0.73101(9)	43(2)	75(3)	54(2)	30
Sc	2*a*	¾	¼	0	68(4)	41(6)	58(3)	296
					23(4)	4(6)	17(3)	30

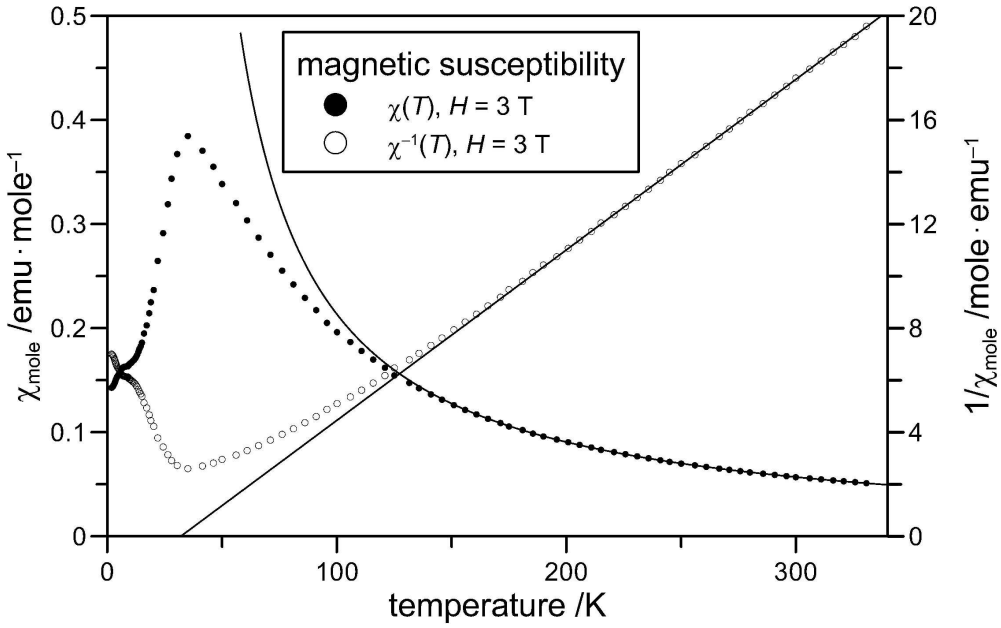

Figure 1. Susceptibility and inverse susceptibility of ScDySb versus temperature.
192x119mm (600 x 600 DPI)

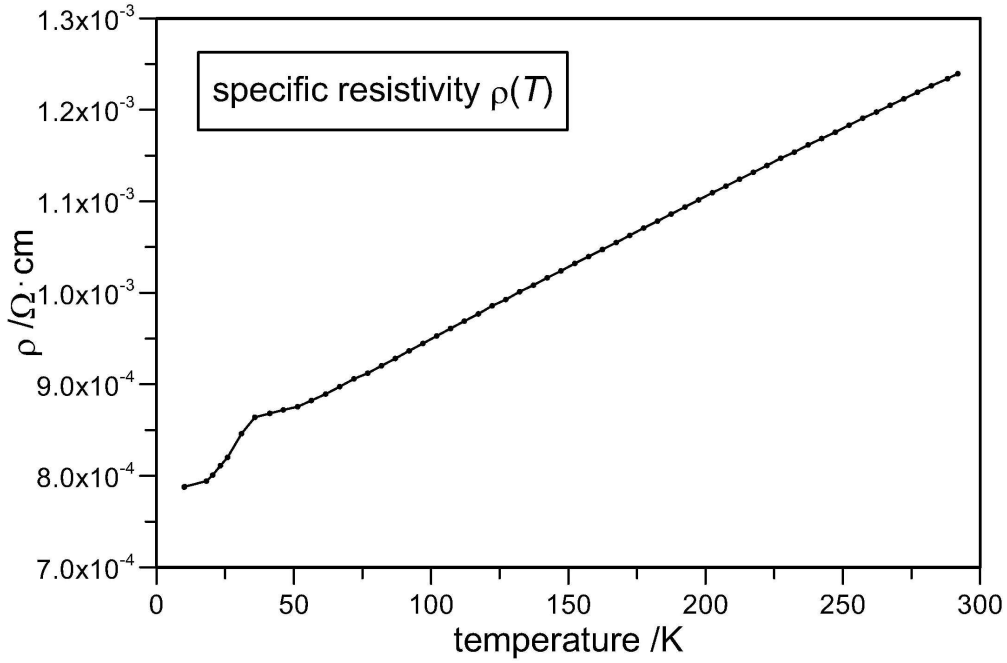

Figure 2. Electric resistivity vs. temperature of ScDySb, between 5 and 295 K.
182x120mm (600 x 600 DPI)

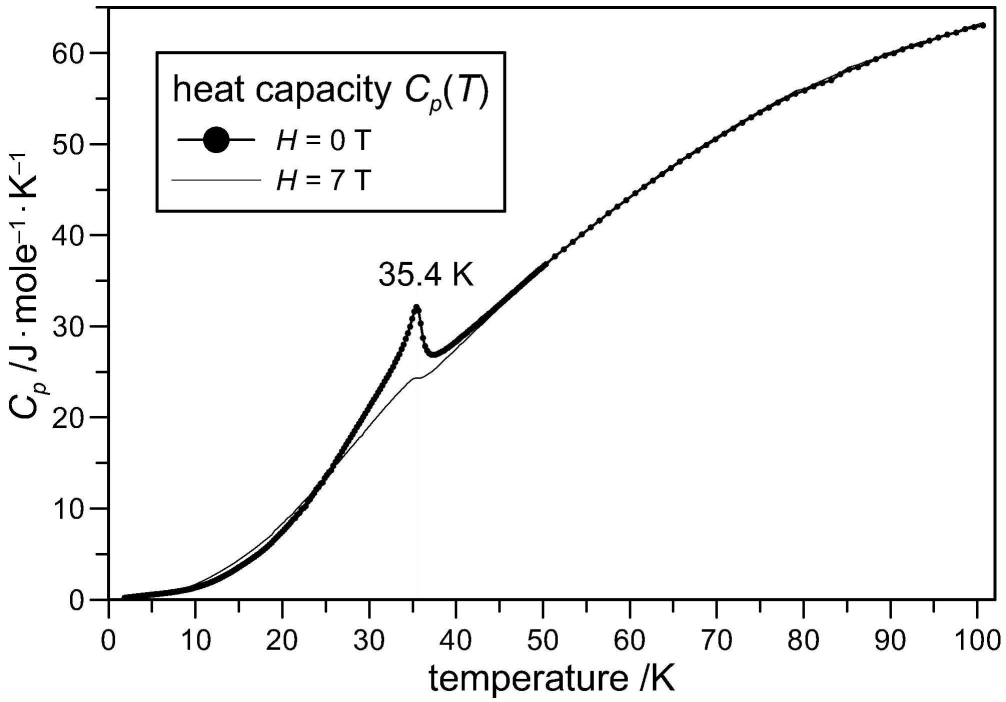

Figure 3. Heat capacity of SyDySb, between 2 and 100 K.
168x117mm (600 x 600 DPI)

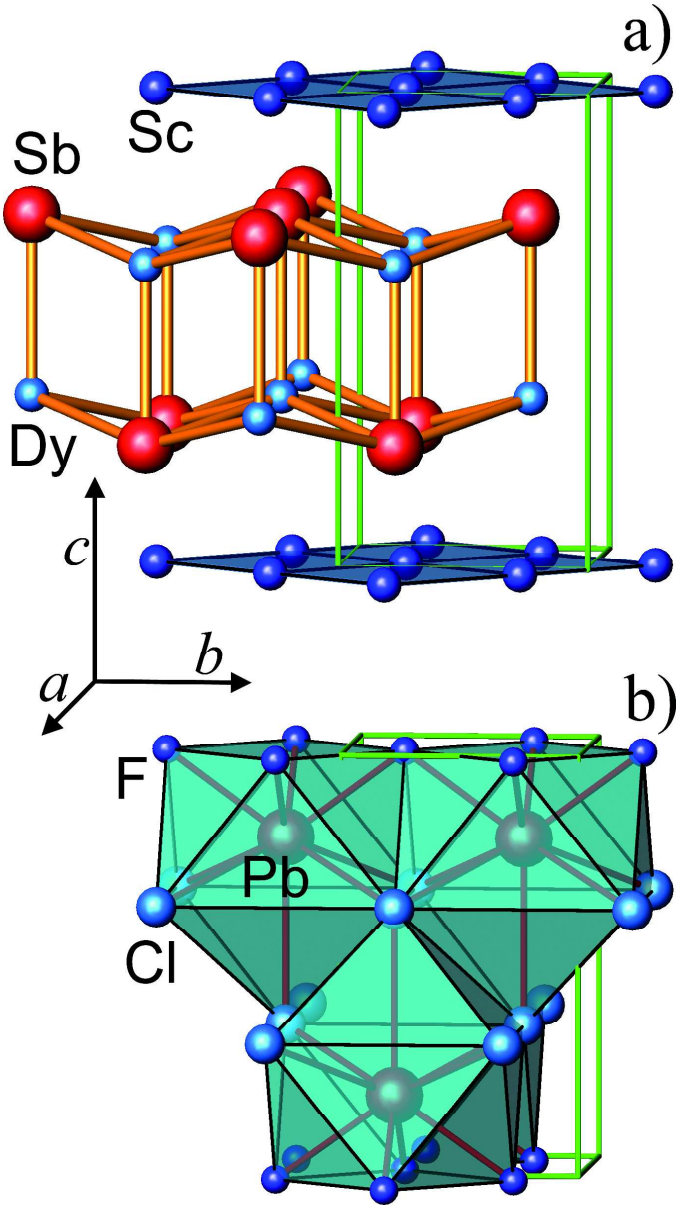

Figure 4. Perspective representation of the crystal structures of a) ScDySb and b) PbFCl. The margins of the unit cell are shown in green, [37].
115x206mm (600 x 600 DPI)

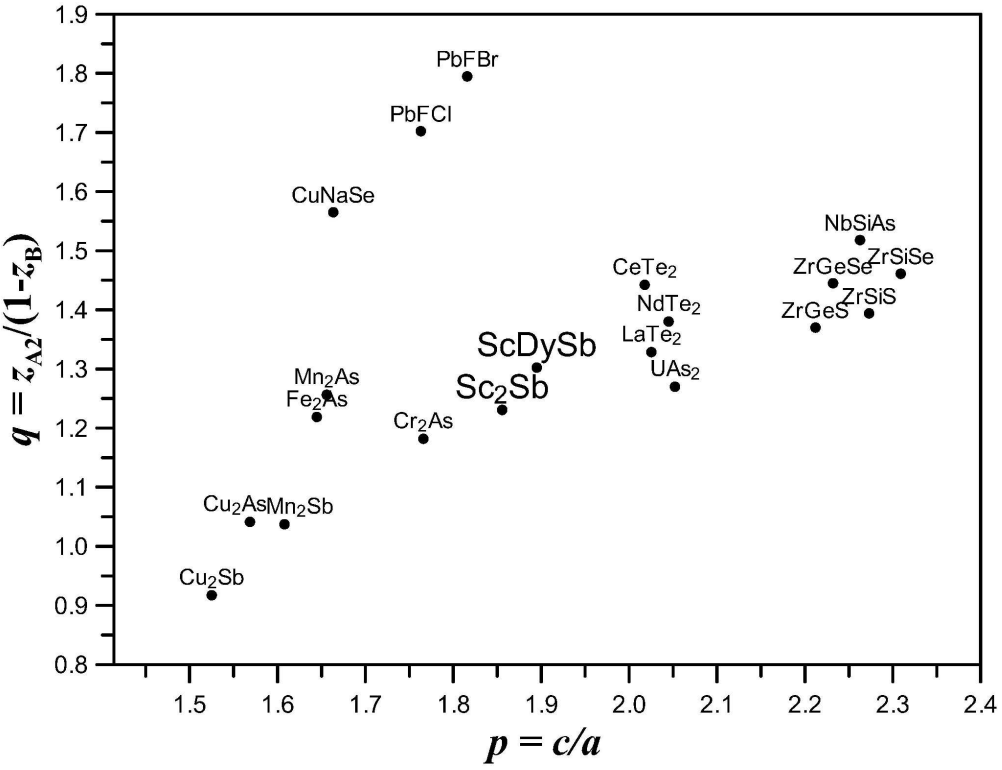

Figure 5. Structure map, showing selected A_2B compounds. The function $z_{A2}/(1-z_B) = f(c/a)$ visualizes the structural distortion (data from [9-11, 16]).
173x132mm (600 x 600 DPI)

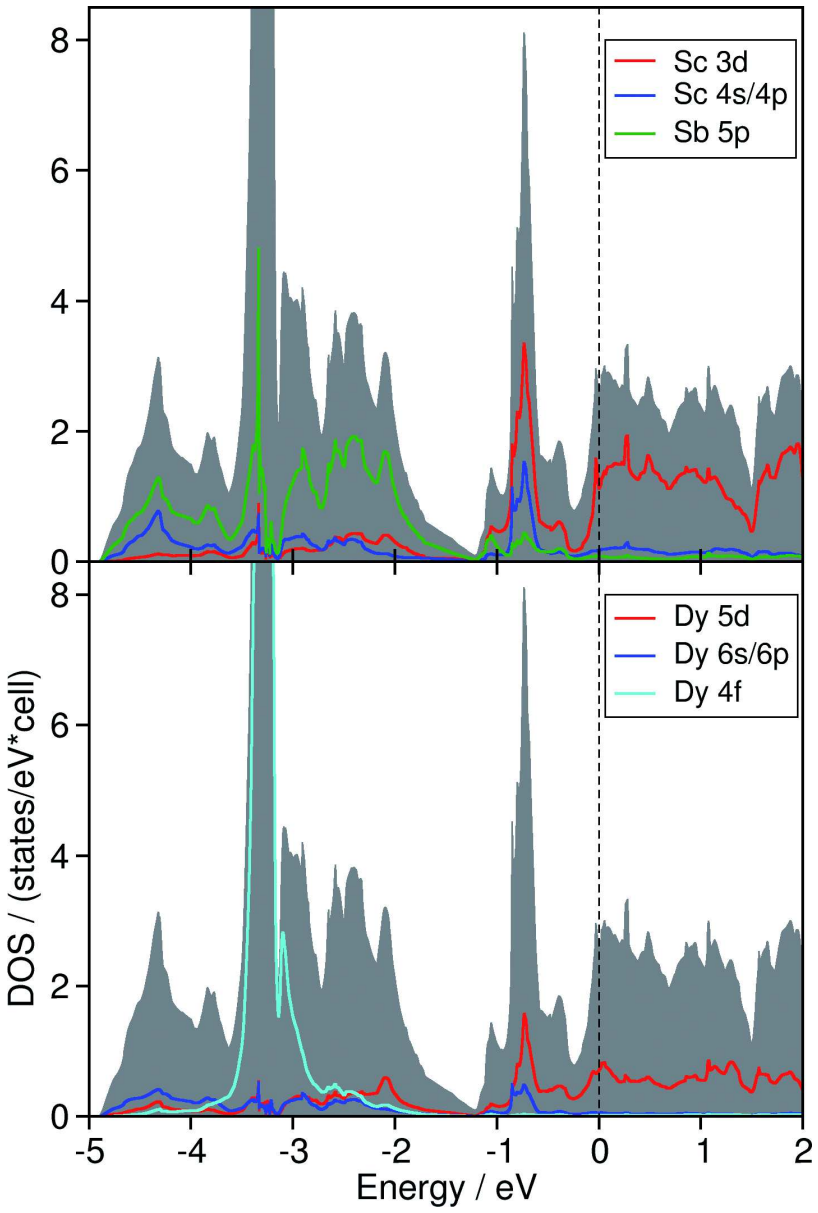

Figure 6. Total (grey area) and projected densities of states (see legend) of the majority spin component of ScDySb. The Fermi level (EF) is shifted to 0 eV.
121x181mm (300 x 300 DPI)

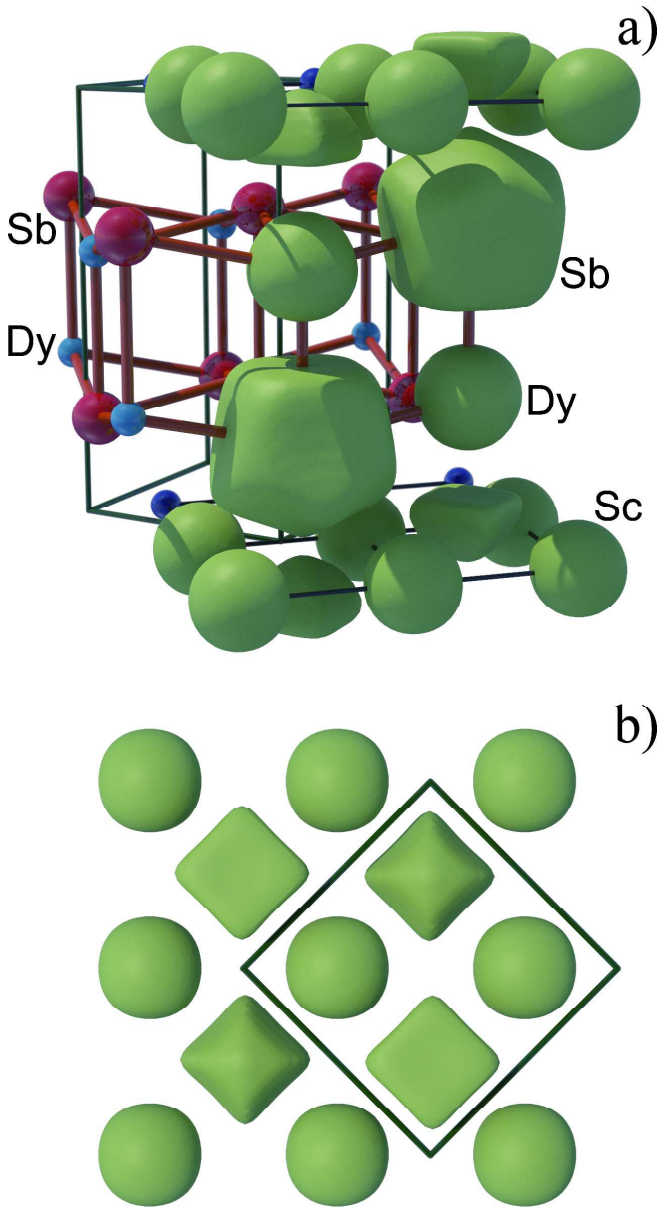

Figure 7. Domains of the Electron Localization Function (ELF, η = 0.5) in ScDySb, a) perspective representation of the crystal structure, b) Sc-layer perpendicular to the c-axis.
108x201mm (600 x 600 DPI)